Journal of Coastal Research	12	4	969–976	Fort Lauderdale, Florida	Fall 1996

Multispectral Video Measurements Over the Chesapeake Bay

T. Niedrauer†, C. Paul†, J. Zaitzeff‡ and P. Clemente-Colon‡

†Xybion Corporation
240 Cedar Knolls Road
Cedar Knolls, NJ 07927,
U.S.A.

‡NOAA/NESDIS
Ocean Sciences Branch
World Weather Building,
Room 102
Code E/RA13
Washington, D.C. 20233,
U.S.A.

ABSTRACT

NIEDRAUER, T.; PAUL, C.; ZAITZEFF, J., and CLEMENTE-COLON, P., 1996. Multispectral video measurements over the Chesapeake Bay. *Journal of Coastal Research*, 12(4), 969–976. Fort Lauderdale (Florida), ISSN 0749-0208.

NOAA's Airborne Multispectral Measurement System (AMMS) is compared to NASA's Airborne Oceanographic Lidar (AOL) with its integral passive ocean color subsystem (POCS) by analyzing a data set collected in April 1991 over the Chesapeake Bay. In this remote sensing experiment, the AMMS and AOL were mounted on a NASA P3 aircraft that flew two passes over a study region at an altitude of 150 m, while a ship collected sea surface samples. The AMMS included a 6 channel multispectral video camera and upward and downward looking spectrometers. The AOL used a laser operating at 532 nm and a 32 channel passive radiometer. A ship gathered sea surface samples, which were analyzed for chlorophyll-a, pheophytin, and seston. The remote sensing measurements from the instruments were in good agreement when the effects of different sampling times and the different sampling areas are taken into consideration.

ADDITIONAL INDEX WORDS: *Remote sensing, imaging, airborne sensors.*

INTRODUCTION

This experiment was part of a multidisciplinary study of the Chesapeake Bay to evaluate the AMMS for measurement of chlorophyll-a variations in coastal waters. It also provided the first comprehensive experimental basis for comparison of the performance of the AMMS with that of another airborne remote sensing system. The AMMS combines an Intensified Multispectral Video Camera (IMC) with a PC computer that is used for IMC control and for data analysis. The System also includes a spectroradiometer, a S-VHS videocassette recorder, video monitor, and power distribution system all designed for use in field experiments conducted from small aircraft for detection and classification applications. The system provides high spatial and spectral resolution image data in six narrow (*e.g.* ±10 nm) user defined bands in the 400–900 nm wavelength region. The high sensitivity of the camera allows the use of narrow-band filters for highly specific measurement algorithms. A detailed description of the AMMS specification is provided by FROST (1990).

The use of video data for water quality and aquatic vegetation monitoring is not common, though interest in the technology for environmental and research applications is rapidly increasing. Video camera applications and fundamentals have been described by MEISNER (1986), HAME (1988), NIEDRAUER (1991), and MAUSEL *et al.* (1991).

The AMMS was developed by the Xybion Corporation for NOAA to address data requirements for coastal marine parameters that vary rapidly in time and space. Specific parameters of estuarine and near-shore waters need to be measured synoptically and accurately for improving the understanding and prediction of coastal dynamics. Remote sensing methods provide the capability of making the synoptic observations necessary for addressing the coastal dynamics and their mechanisms. As a result, satellites have been successful in observing various large scale color and thermal features in the open ocean. However, estuaries and their associated coastal waters have more stringent spatial, spectral, and temporal resolution requirements than the open ocean. For instance, spatial resolution requirements for estuarine studies can be as small as 5–50 meters, as compared to 1–10 km for the open ocean. Similarly, temporal coverages of every 3–6 hours may be required, as compared to 1–7 days for the open ocean. These requirements have led to the development of a low-cost airborne system to complement satellite and *in-situ* measurements.

METHODS

Instrumentation

The remote sensing systems used in the field experiment are the AMMS and the AOL/POCS. The primary new sensor used in this study was the IMC, whose characteristics relevant to the experiments are summarized in the following section. The AOL/POCS's characteristics are described in detail

94112 received and accepted in revision 9 June 1994.

Table 1. *Characteristics of the NOAA narrowband filters for IMC. The last column has typical exposure times for the April 26 experiment over Chesapeake Bay.*

IMC Filter Characteristics			
Wavelength (nm)	Bandwidth (nm)	Peak Transmissivity (%)	Exposure Time (ms)
412	9	43	2.5
442	11	60	0.5
490	12	65	0.2
521	11	60	0.15
560	11	62	0.12
660	9	74	0.30

in HOGE and SWIFT (1986, 1983, 1981a,b) and HOGE *et al.* (1986), and are briefly summarized here.

Intensified Multispectral Camera (IMC)

The IMC uses a standard C-mount lens with a rotating filter wheel behind it. The filter wheel, which holds 6 narrowband interference filters, rotates synchronously with the video scanning rate at 300 rpm. The light passing through a filter hits a multichannel plate image intensifier that is coupled with fiber optics to a charged couple device (CCD) image array. The image intensifier provides the gain needed to allow use of narrowband filters. The intensifier's power supply is used as an electronic shutter to control the amount of light reaching the CCD. Typical exposure times for nominal 10 nm filters and a 70% camera gain setting are shown in Table 1, which also shows the characteristics of the filters selected for chlorophyll measurement. The IMC's range of possible exposure times is 0.05 μsec to 4,000 μsec.

The images from the IMC are encoded into an RS-170 video format and recorded on a S-VHS VCR for later analysis; these images may also be sent directly to the system computer for immediate digitization and analysis. The images are typically digitized into a 752 horizontal by 480 vertical array of pixels. Each pixel consists of an 8 bit digital number (DN) with a value between 0 and 255, which represents the brightness of the image at that location. The exposure time, camera gain, CCD array temperature and other user-specified system parameters are encoded into the video format and are automatically decoded by the system computer.

Testing and Calibration

A number of tests were done to establish the operating characteristics of the IMC. The resolution of the IMC was measured by obtaining the Modulation Transfer Function (MTF) of the camera without any filters in the light path. The MTF was obtained by monitoring the output of the camera with an oscilloscope while the camera imaged a standard (EIA) resolution chart. Figure 1(a) shows the limiting resolution to be about 530 pixels across the horizontal field of view. The 3% modulation point on the MTF curve is normally considered to be the limiting resolution in video specifications. These resolution measurements were made at both high gain and normal gain settings with essentially the same results. The resolution of the IMC is closely matched by the resolution of the VCR.

Another important test conducted on the IMC was the linearity of its output as a function of the input light level. The IMC response at a constant gain level was recorded as a function of known light intensity. The light was obtained from a calibrated integration sphere. Figure 1(b) shows a linear out-

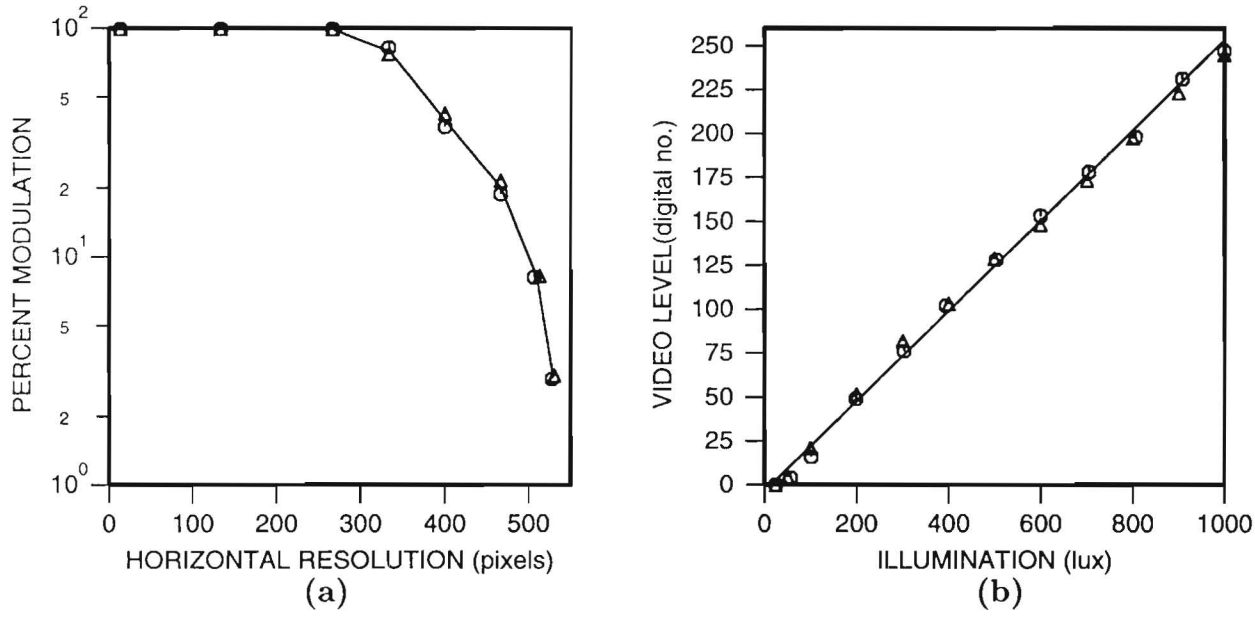

Figure 1. (a) The modulation transfer function for the IMC without any filters. (b) The IMC response to a series of known light levels.

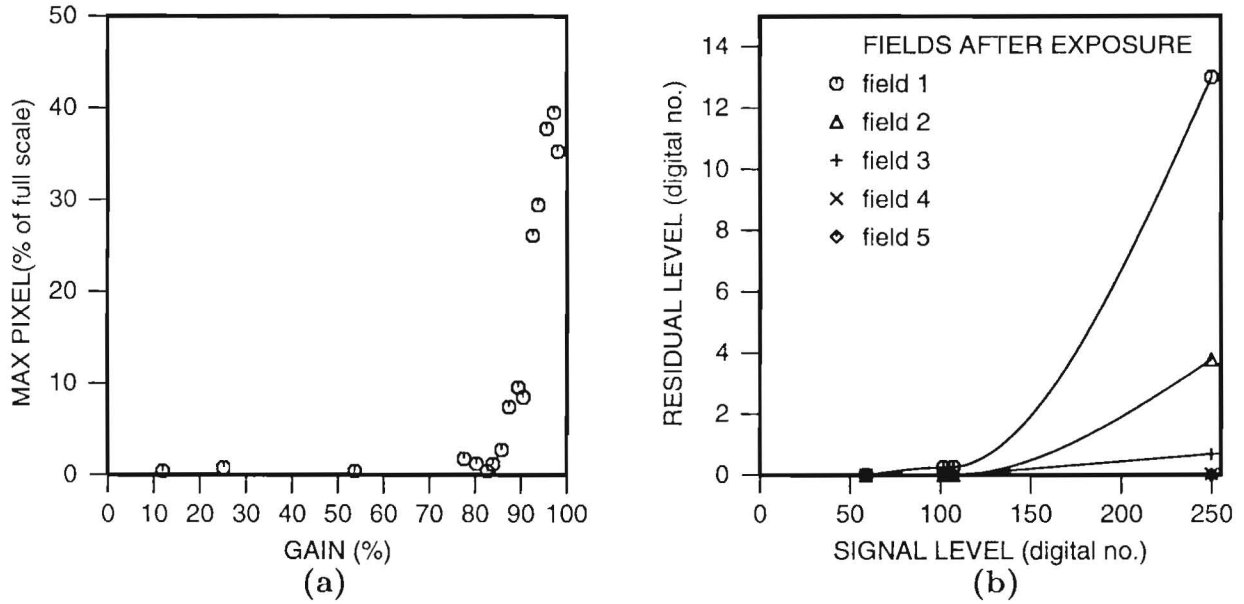

Figure 2. (a) The IMC response (scintillation noise) as a function of gain for no light input. (b) IMC lag as a function of signal level. Each image consists of two fields. There are a series of 12 fields in a 6 filter cycle.

put response over 3 orders of magnitude of input light level variation.

The intensifier tube used in the IMC is subject to scintillation noise and image retention (commonly referred to as 'lag' in video specifications). Scintillation noise is the spontaneous emission of electrons; the level of such emissions depends on the voltage levels applied to the tube, and consequently depends upon gain. As a worse-case test, the IMC integration time was set to 4 msec, the longest possible exposure time, and the lens was covered. A region comprising approximately 20% of the full image located in the center of the resulting image was analyzed and the largest DN was recorded. This was done at a variety of gain settings. As seen in Figure 2(a), the scintillation noise was not significant until the gain levels exceed 85% of the maximum gain.

A test to measure lag was done by exposing the frame of one filter to light and leaving the frames for the other filters unexposed. Thus, light reaches the CCD sensor for only one of every six frames. Ideally, this should result in the exposed filter having an appropriate DN, while leaving all other frames with a digital value of zero. This test was done by setting the exposure time for filter 1 to the longest possible exposure time in the run mode (4 msec) and setting the exposure time for all other filters to the shortest possible time (50 nsec). The IMC was focused on a white reflectance panel, and an Osram high intensity projector light source was adjusted to obtain different intensities. The camera was operated in a frame mode, so that fields 1 and 2 were exposed at the same time through filter 1. The response of the IMC to the remaining filters should ideally have registered a zero light response. This was confirmed by reducing the exposure time in filter 1 to 50 nsec, the minimum exposure time. The light level in all fields then registered zero. The average light intensity recorded in the individual fields following the exposed frame was measured. Figure 2(b) shows negligible residual values for light levels below 110 DN. This means lag should not be a significant issue when the IMC is operated at an average exposure level of 100 DN. However, if the field of view is exposed to higher light levels, then the following frame may have a residual signal. A calibration of this effect would allow for a post-analysis correction of intensity values.

The operator has control over exposure time, gain, and lens settings for the IMC. In addition, the center wavelength and bandwidth of each filter needs to be selected for each application. For airborne remote sensing, aircraft altitude and speed, as well as field of view (lens focal length), need to be specified for each particular data collection exercise. Each of the operator-determined settings is discussed in the following subsections.

Exposure Time

The exposure time is controlled and monitored by one of the microprocessors within the camera. An experiment was done by imaging a constant light source with the IMC and varying the exposure time. The average digital value in a 100 by 100 pixel region in the center of the image was shown to be linear as a function of exposure time.

Gain

The light intensity at the CCD array varies logarithmically with gain in the IMC. Figure 3 shows the log of intensity as a function of gain for the Osram light source. Using the 10 nm bandwidth filters, the camera was operated at gain levels

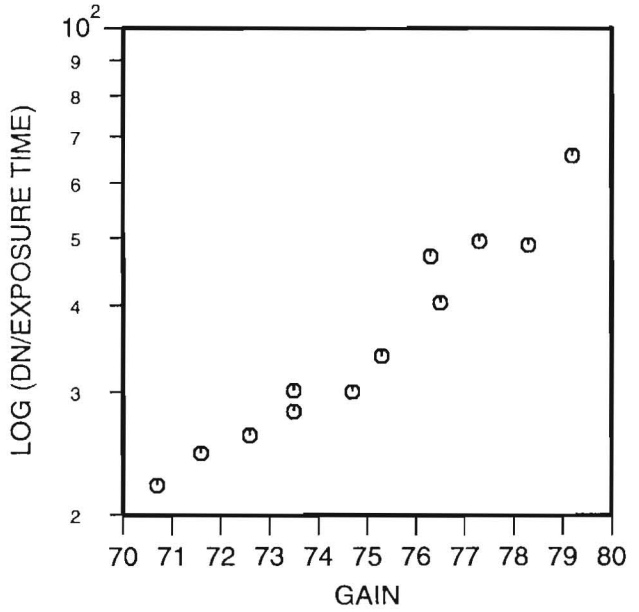

Figure 3. Value measured by the IMC as a function of gain for a constant light source. The y axis has a logarithmic scale of the digital IMC number divided by the exposure time.

below 80% to assure that the scintillation noise was not a problem.

Lens Settings

The focal length and f/number setting of the lens affect the performance of the IMC and must be selected appropriately for each application. The most obvious effect of the lens is on the angular field of view (FOV) of the IMC. The focal length of the lens and the size of the active area on the photocathode determine the FOV. As the FOV increases, the angle of incidence for light rays from an object at the edge of the image increases. Interference filters are usually specified for light passing through them at normal incidence. As the incidence angle increases, the passband gets shifted to shorter wavelengths. The shift decreases with an increase in focal length and incidence angles. It also decreases as the f-number gets larger. The following equation describes the change in center wavelength CWL, with focal length F_L, f stop f/, and refractive index N_e.

$$CWL_F = CWL_N \frac{\sqrt{N_e^2 - \sin^2(\theta)}}{N_e}. \quad (1)$$

The subscript N refers to normal incidence, while θ is the angle of incidence of the filter (half of the angular field of view).

$$\sin(\theta) = \frac{Q}{\sqrt{Q^2 + F_L^2}} \quad (2)$$

$$Q = \frac{H + \frac{F_L}{f/}}{2} \quad (3)$$

The effective width, H, of the intensified CCD imager is 12.7 mm horizontal and 9.5 mm vertical for the IMC's video format.

AMMS Spectrometers

The AMMS has a 256 channel spectrometer for taking point (non-image) measurements. For this trial, two collection heads were attached to the system, one pointed upward with a cosine collector for irradiance measurements and the other pointed downward with a slit collector for radiance measurements. The integration times for these instruments could vary from 1/60 sec to 64/60 sec. Collection of data from either of these heads is controlled by the operator.

AOL

NASA's AOL has been described in detail in other papers discussing chlorophyll mapping (HOGE and SWIFT (1986) and HOGE *et al.* (1986, 1983, 1981a,b)) in oceanic regions. The AOL has a laser that emits light at 532 nm and causes plankton to fluoresce at 685 nm. The laser has a pulse rate of 6.25 Hz. The receiver is a 32 channel collection of photomultiplier tubes. The bandwidth of each tube is 11.25 nm and together the 32 tubes span a contiguous spectral region from 365–725 nm. The integration time of the tubes is 0.2 msec. The sampling rate is 12.5 Hz so both active and passive spectra are obtained. The raw samples are averaged over 14 samples in preliminary processing.

Calibration

A calibration of the AMMS was obtained at the NASA Wallops Island Flight Facility using a 76 cm integration sphere operated by NASA. The IMC and both spectroradiometers were calibrated. The AOL is routinely calibrated before and after each flight.

The AMMS instruments had a linear response as the integration sphere light level was varied. The IMC and the downward looking spectroradiometer were 8 inches from the output port of the integration sphere. There were 7 radiance levels, I, recorded by the IMC and the downward looking spectroradiometer. There were only 3 irradiance levels recorded by the upward looking spectroradiometer. A linear regression between the IMC values and the calibrated irradiance had a coefficient of determination, r^2, of better than 0.995 for each of the six filters. The following equations calculate the irradiance, from the values recorded by the IMC or spectroradiometer.

$$I = m \times V_{IMC} + b \quad (4)$$

$$I = m_1 \times V_{SP} + b_1 \quad (5)$$

$$I = m_2 \times V_{SP} + b_2 \quad (6)$$

The DN recorded by the IMC is divided by the exposure time in milliseconds to get V_{IMC}. The DN from the spectroradiometer is multiplied by 64 and divided by the integration time in 60th's of a second to find V_{SP}. The regression coefficients, m and b, are listed in Table 2.

Table 2. *Regression coefficients for IMC, downward looking spectroradiometer, and upward looking spectroradiometer.*

	AMMS Regression Coefficients Center Wavelength (nm)					
	412	440	490	521	560	660
			IMC			
m	0.0167	0.0033	0.0016	0.0015	0.0016	0.0016
b	−0.11	0.03	−0.02	0.01	−0.08	0.27
			Downward Spectroradiometer			
m_1	0.00100	0.00078	0.00066	0.00060	0.00057	0.00057
b_1	−0.0047	−0.0006	0.0149	0.0144	0.0306	0.0676
			Upward Spectroradiometer			
m_2	0.0078	0.0038	0.0029	0.0026	0.0022	0.0020
b_2	0.12	0.06	0.08	0.08	0.04	0.18

RESULTS

The test area for this experiment comprised the north central region of the Chesapeake Bay between latitudes 38°20′ and 39°00′ north, as shown in Figure 4. The P3 entered the study area at 9:40 EST. It flew north, turned around, and retraced the track, leaving the study area at 10:26. The jerkiness in the P3 flight path is an artifact of the position measuring system in normal operation (Figure 4). These jumps in position can be as much as 200 m. The AMMS and AOL both gathered data during this flight. During the experiment the Bay was dominated by a high variability of chlorophyll concentrations. Shipboard measurements ranged from 3.0 to 160 μgrams/liter.

The ship took chlorophyll samples at 22 stations (Figure 4) and concurrent seston samples at 14 of the stations. The ship stations occurred between 08:28 and 14:58.

While the ship and P3 did have two simultaneous stations, the stations were not in exactly the same spot. The patchiness of the chlorophyll did not allow a reasonable comparison. One significant patch of chlorophyll detected by the P3 AOL was 400 m in length. The corresponding ship station was 1200 m away, with a time lag of less than 1 hour from the time the P3 flew by. The ship data did not show a high chlorophyll region.

When the sea-surface samples were repeated at about the same location on the return leg, the chlorophyll peaks shifted (Figure 5). The lack of repeatability may be due to advection of the water masses and the lack of sampling in the same position.

DISCUSSION

Several studies (CAMPBELL and ESIAS, 1983 and HOGE and SWIFT, 1986) have shown a relation between the inflection ratio, G, and chlorophyll concentration, C. The inflection ratio algorithm is:

$$\log(C) = b + mG \tag{7}$$

$$G = \frac{I_p I_p}{I_m I_n} \tag{8}$$

The radiances, I_m, I_p, and I_n, are measured at wavelengths of 441 nm, 490 nm, and 521 nm respectively, using approxi-

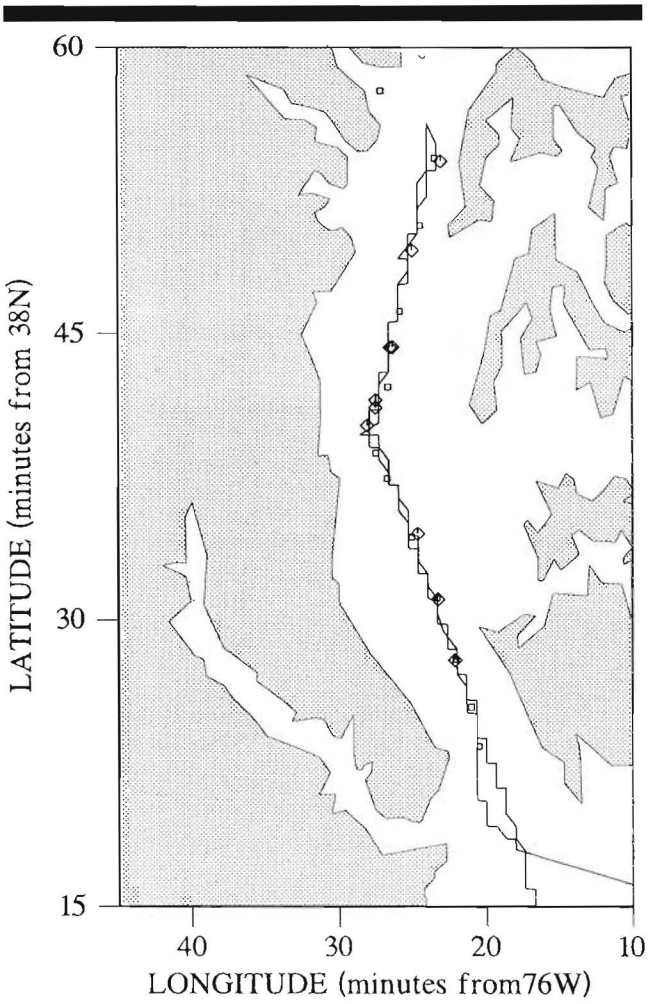

Figure 4. Ship track (□ is N-S leg and ◇ is S-N return leg) and plane track (lines) for 26 April 1991.

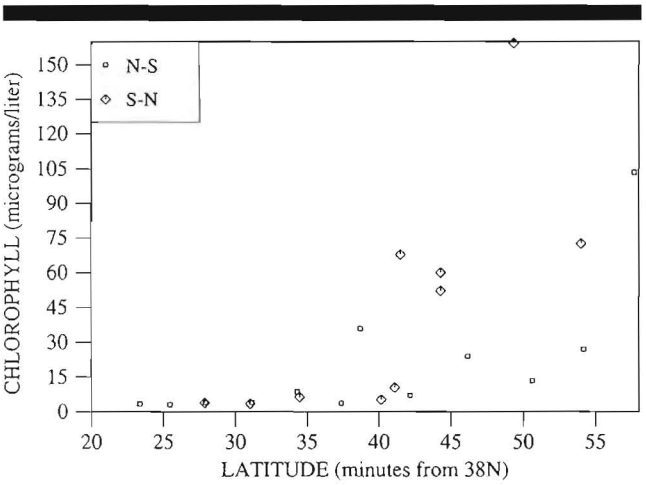

Figure 5. The sea-surface chlorophyll values measured from the N-S and S-N passes of the ship through the study area.

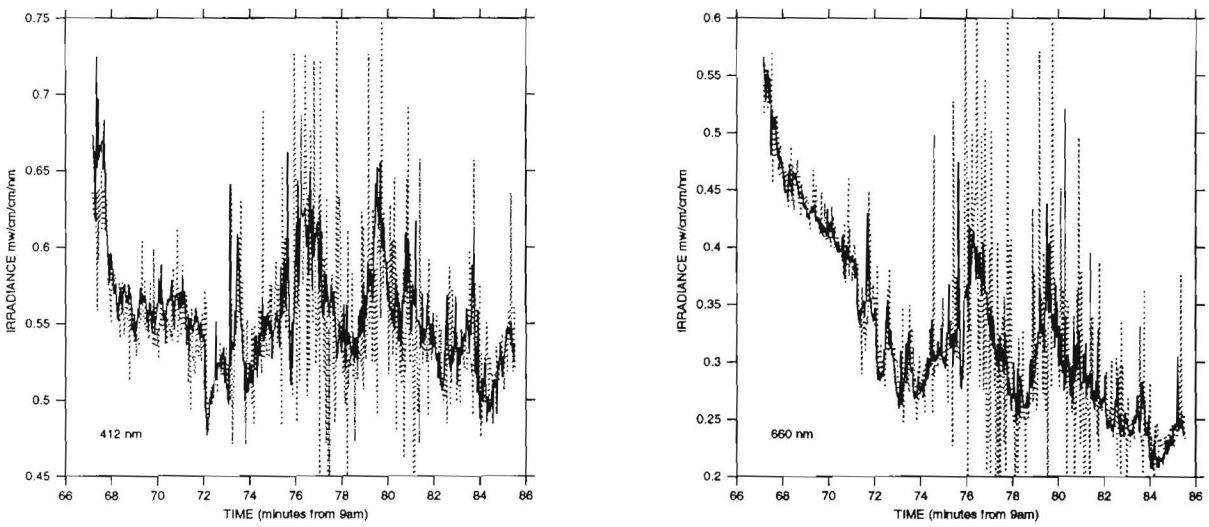

Figure 6. P3 flight line with IMC and passive radiometer data for two wavelengths. This 120 km north to south flight line was sampled in 20 minutes. The IMC values (solid lines) are irradiances, while the radiometer values (dotted lines) have been fit to the IMC values with a linear regression.

mately 10 nm wide filters. An earlier study (HOGE and SWIFT, 1986) applied the inflection algorithm to open ocean data with concentrations up to 3 μg/l and got correlation coefficients above 0.9, although there were regions where the algorithm did not produce a good fit.

For chlorophyll in fresh water, DIERBERG *et al.* (1994) tested several algorithms using AMMS data and showed R^2 values of up to 0.95. Among the algorithms tested were a ratio of the reflectances of 700 to 680 nm and a line height algorithm (LHA):

$$\mathrm{LHA} = (E_i - E_{i+1}) - \frac{CWL_i - CWL_{i+1}}{CWL_{i-1} - CWL_{i+1}}(E_{i-1} - E_{i+1}) \quad (9)$$

where E_i is the spectral energy and CWL_i is the center wavelength of band i. Both of these algorithms had some success. The fresh water algorithms cannot be applied to this experiment because they used wavelengths outside of the range of wavelength available in this coastal experiment.

Researchers have had mixed results in relating remotely sensed radiative data to sampled data taken from a ship over a period of hours. A number of projects have had poor results. HARDING *et al.* (1992) took radiative measurements with NASA's Ocean Data Acquisition System (ODAS) and had correlation with an R of 0.668 between ship data and ODAS data using the G algorithm. ODAS is a 3 channel point radiometer with bands at 460, 490, and 520 nm. This covered 73 stations taken in 1989 in the Chesapeake Bay. A study using NASA's AVRIS (CARDER *et al.*, 1993) and flown on an ER-2 in the Tampa Bay region indicated that bottom features can have a significant effect on upwelling radiances. Though they did not present any of their chlorophyll data, they stated that bottom effects would cause ratio algorithms to suffer some distortion. They also had to spatially average regions of up to 1 km to get a sufficient signal to noise ratio (SNR) at the shorter wavelengths (415 nm).

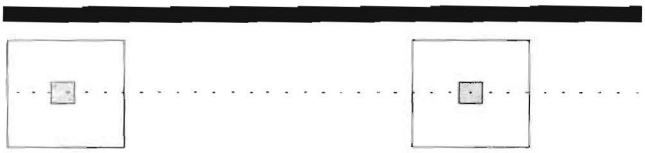

Figure 7. Size of viewing regions for IMC (large squares) and NASA passive radiometer (small dashes). The size and spacing for the IMC sample region was chosen during postprocessing and is shown by the shaded square within each IMC viewing area.

The AMMS tests have been important for developing techniques to collect data and to analyze the data. The analysis efforts for this project have focused on comparing the IMC measurements to the AOL and on comparing the IMC measurements to sea surface samples. The comparison with other instruments has shown the effects of different integration times and differing spatial scales. The irradiances measured by the AMMS are well correlated with the values recorded from NASA's passive radiometer in regions where the radiance is smoothly varying. Figure 6 shows the IMC values for a 20 minute flight segment over Chesapeake Bay.

The corresponding passive radiometer values are also plotted. Calibration coefficients for the radiometer values are not available, so a linear transformation was applied to match them to the IMC values. The calibration for the radiometer channels is just a linear correction, so the similarity between NASA's radiometer and the IMC will remain after calibration.

The spatial and temporal scales are different for the two sensors. The IMC has exposure times of 0.1–2.5 msec and views a region about 50 m by 50 m. The area of interest chosen for the IMC in postprocessing was about 10 m by 10 m. This was chosen so the shadow of the aircraft was not in the area of interest. Also, sun glint was minimized by choosing

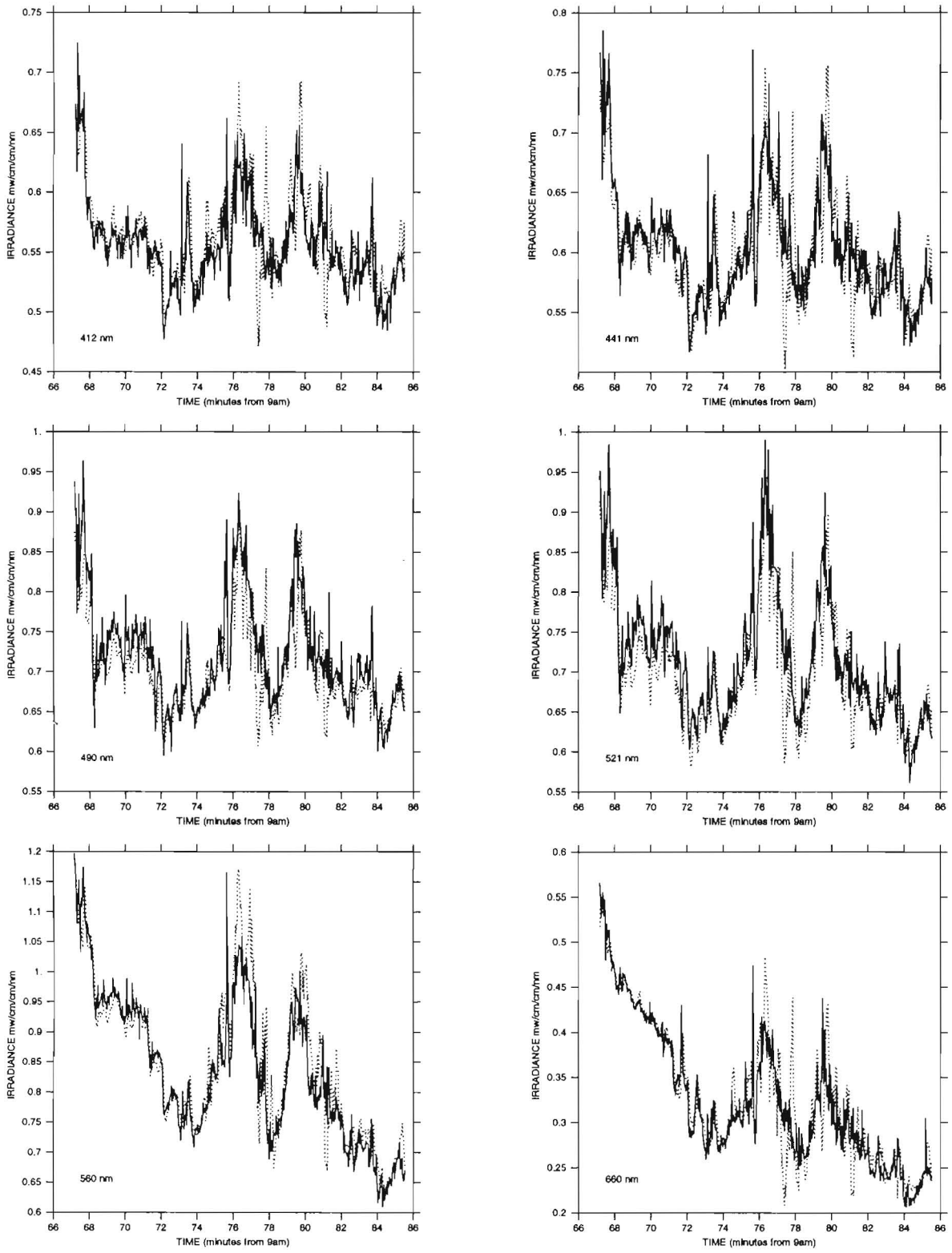

Figure 8. P3 flight line from north to south with IMC and passive radiometer data at all six wavelengths. The IMC values (solid lines) are irradiances, while the radiometer values (dotted lines) have been linearly fit to the IMC values and averaged over 5 points.

the center of the field of view, rather than the edges. For one flight segment, a bright region was observed in the center of the airplane shadow, approximately where the laser was located. The IMC lens was not in focus for this flight and resulted in a blurred image. The blurriness of the images causes smaller AOI regions to have the same characteristics as the larger region. The total area analyzed in an IMC image is about 100 m^2. The AOL radiometer was looking at a 0.3 m by 1.2 m region for a 0.2 msec time period. Therefore, the radiometer will detect much smaller features than the IMC. Each AOL radiometer value was an average of 14 samples, so the area viewed by the radiometer is 5.4 m^2. Thus, the radiometer should detect spatial features 18 times smaller than the IMC. As a direct result of this sampling, the AOL radiometer has a more variable signal than the IMC.

Figure 6 has IMC values every 1.8 sec and radiometer values every 1.1 sec. The sampling rate of the radiometer was established by averaging 14 samples before data was stored during the experiment. The sampling rate for the IMC was set by having the system computer analyze images at a rate comparable to the radiometer rate. The relative size and position for the sampling areas are shown in Figure 7. The IMC data corresponds to a 10 m square every 180 m along the flight path while the radiometer data contains 14 rectangles (0.4 m^2) spaced every 8 m along the flight path. On average, one of the radiometer rectangles will be in the IMC square.

The IMC and NASA radiometer measurements became very similar when a 5 point running-mean filter was applied to the radiometer data. The resulting series is shown in Figure 8. The 560 m strip along the flight path measured by NASA's radiometer has a mean similar to the IMC's 10 m square.

With the different sampling areas, it is understandable that the IMC and AOL have no correlation in regions where patchiness is present. However, in regions of smooth transitions, correlations increase. For instance, in the 660 nm band for the first 5 minutes of the N-S leg, the correlation (r^2) is 0.62.

CONCLUSION

Two different remote sensing instruments have collected radiance data over an estuary. Given the different sampling footprints, the time series data from the two instruments are very similar. The AMMS, with its IMC, provides a relatively wide swath for 6 channels. The AOL POCS provides 32 channels of radiance data from a narrow footprint.

The AMMS is a low-cost imaging instrument suitable for estuarine monitoring. With calibration, it can provide radiative measurements comparable to the AOL's POCS subsystem. Since the AMMS can be flown from a small single-engine plane, it should prove to be a versatile, cost-effective tool for the collection of radiative data.

LITERATURE CITED

CAMPBELL, J. and ESAIAS, W., 1983. Basis for spectral curvature algorithms in remote sensing of chlorophyll. *Applied Optics*, 22(7), 1084–1093.

CARDER, K.; REINERSMAN, P.; CHEN, R., and MULLER-KARGER, F., 1993. AVRIS Calibrations and application in coastal oceanic environments. *Remote Sensing Environment*, 44, 205–216.

DIERBERG, FORREST, E. and CARRIKER, NEIL E., 1994. Field testing two instruments for remotely sensing water quality in the Tennessee Valley. *Environmental Science & Technology*, 28(1), 16–25.

FROST, P., 1990. Discrimination and classification with Xybion multispectral video system. *19th International Congress on High Speed Photography and Photonics* (Cambridge, England), 16–21 September 1990.

HAME, T. and RANTASUO, M., 1988. Shuttered camera—Aerial color video imaging in the visible and near infrared. *Photogrammetric Engineering and Remote Sensing*, 54(12), 1735–1738.

HARDING, L.; ITSWEIRE, E., and ESAIAS, W., 1992. Determination of phytoplankton chlorophyll concentrations in the Chesapeake Bay with aircraft remote sensing. *Remote Sensing Environment*, 40, 79–100.

HOGE, F. and SWIFT, R., 1986. Chlorophyll pigment concentration using spectral curvature algorithms: An evaluation of present and proposed satellite ocean color sensor bands. *Applied Optics*, 25(20), 3677–3682.

HOGE, F.; BERRY, R., and SWIFT, R., 1986. Active-passive airborne ocean color measurement. 1: Instrumentation. *Applied Optics*, 25(1), 39–47.

HOGE, F. and SWIFT, R., 1983. Airborne dual laser excitation and mapping of phytoplankton photopigments in a gulf stream warm core ring. *Applied Optics*, 22, 2272+.

HOGE, F. and SWIFT, R., 1981a. Application of the NASA Airborne Oceanographic Lidar to the mapping of chlorophyll and other organic pigments. *Chesapeake Bay Plume Study Superflux 1980*, Nasa Conference Publication 2188 (U.S. GPO, Washington, D.C., 1981), pp. 349–374.

HOGE, F. and SWIFT, R., 1981b. Airborne simultaneous spectroscopic detection of laser-induced water raman backscatter and fluorescence from chlorophyll a and other naturally occurring pigments. *Applied Optics*, 20, 3197+.

MAUSEL, P.; KARASKA, M.; MAO, C.; ESCOBAR, D., and EVERITT, J., 1991. Insights into secchi transparency through computer analysis of aerial multispectral video data. *International Journal Remote Sensing*, 12(12), 2485–2492.

MEISNER, D., 1986. Fundamentals of airborne video remote sensing. *Remote Sensing of the Environment*, 19, 63–79.

NIEDRAUER, T., 1991. A coastal survey with a multispectral video system. *In*: CURRAN, R., SMITH, J., and WATSON, K., (eds.), *Earth and Atmospheric Remote Sensing*, Proceedings SPIE 1492, 240–251.